



Tanker Wake Effects on the Trailing UAV in Autonomous Aerial Refueling

D. Zhang¹, Y. Chen^{1†} and X. H. Fu²

¹ Air Force Engineering University, Xi'an 710038, China

² Air Force 93413, Shijiazhuang 050000, China

†Corresponding Author Email: cheny_043@163.com

(Received January 6, 2019; accepted July 17, 2019)

ABSTRACT

Autonomous aerial refueling is a typical close formation flight process, in which the tanker wake has a strong aerodynamic influence to the receiver. In order to develop the accurate aerodynamic models in refueling simulations and design the control laws for autonomous aerial refueling, the tanker wake effects on an Unmanned Aerial Vehicle (UAV) are investigated through ANSYS CFX 15.0. A simplified boom-equipped tanker and a tailless delta wing UAV (named ZD-X) are used in this study. The aerodynamic characteristics of ZD-X in single flight are calculated first and the results are used as the benchmark for comparison. Then the aerodynamic characteristics of ZD-X under the effects of tanker wake are calculated, the final results are given in incremental form to facilitate comparative analysis. Numerical results are obtained from the tanker and receiver at varying lateral, vertical and longitudinal spacings. It is observed that the tanker wake effects on the receiver mostly come from wingtip vortices of the tanker wing and horizontal tail, and the lateral and vertical spacings have significant effects on the aerodynamic characteristics of the receiver, while the longitudinal spacing has almost no effect.

Keywords: Autonomous aerial refueling; Aerodynamic influence; Tanker wake effects.

1. INTRODUCTION

Unmanned Aerial Vehicle (UAV) plays a critical role in recent wars and has been widely deployed to perform various military operations ranging from reconnaissance, intelligence acquisition, to combat strike (Anon 2005, Waharte 2010). However, the existing UAVs still have the same problems as manned aircrafts, such as short in range and endurance, lack of flexibility in deployment and limitation of station time on time-critical target. One way to solve these problems is to develop aerial refueling (AR) technology. Refueling operations of the manned aircrafts demand fast reactions and high level of training for the pilots. Even so, a lot of accidents happen in the operations and the success rate of aerial refueling is very low. No pilot operations on the UAVs will make aerial refueling extremely difficult, and it is necessary to adopt autonomous aerial refueling (AAR) technology, which requires accurate position tracking technologies and elegant control strategies. The autonomous aerial refueling is a typical close formation flight process, in which the tanker wake characterized by unsteady, time-varying, and

nonlinear factors has a significant interference on the receiver (Gerza *et al.* 2002, Fravolini *et al.* 2004). Therefore, the primary task of achieving the goal of autonomous aerial refueling is to study the aerodynamic influence from the tanker wake to the receiver in autonomous aerial refueling, which is the basis for wake modeling and control methods design of the trailing UAV.

Bloy and his colleagues used a variety of methods to investigate the influence of tanker wake on the receiver, covering simple horseshoe vortex model, vortex lattice method (VLM) (Bloy *et al.* 1986, 1987, 1990), and flat vortex sheets (Bloy *et al.* 1993). They found that for each combination of receiver and tanker, the aerodynamic loads are mainly affected by the relative lateral position, and the side-wash effect of the tanker wake on the vertical tail of the receiver results in a large side force. Blake *et al.* (2004a, 2004b) studied the aerodynamic influence from the tanker wake to the receiver through wind tunnel tests. Their research showed that the wake interference is dominated by lateral and vertical spacings and weakly by longitudinal spacing. Dogan investigated the tanker

wake effects on the receiver through the flight test (Dogan, *et al.* 2008). They found that the wake vortices of the tanker caused a non-uniform, deterministic and random flow, which brought about changes in the aerodynamic characteristics of the receiver. For the purpose of studying the fuel-saving effect of the F/A-18 aircraft in close formation flight, NASA used two F/A-18 aircrafts to investigate the aerodynamic influence between the two vehicles. The results showed that the if the F/A-18 aircraft kept flying in the ideal position through precise flight control during close formation flight, it would bring about 20% fuel savings owing to the wake effects of the leading F/A-18 aircraft (Vachon, *et al.* 2003).

Although a lot of literatures have studied the tanker wake effects on the receiver, we still need to analyze and model the wake effects for a specific configuration to obtain the corresponding aerodynamic data, which is indispensable for developing analytical models and building the simulation environment. Furthermore, most of the previous studies related to tanker wake influence to receiver adopted analytical modeling methods or test means, which are inconvenient for a thorough analysis and understanding of the flow mechanism and aerodynamic influence due to the complexity of the flow field and the limitation of research methods.

With the development of computational technology, the computational fluid dynamics (CFD) method is widely used in flow field analysis because of its convenience, accuracy and inexpensiveness. The commercial software ANSYS CFX 15.0 will be used to study the tanker wake influence to the receiver in this paper. The most challenging problem in this study is to accurately capture the wake of tanker, which requires refinement of the grids near the wake flow field. Grids refinement will dramatically increase the number of grids, which is a challenge to the computing capabilities. Therefore, a high performance server will be used for numerical calculation in this paper. Then the calculation results will be analyzed by the streamlines, pressure contours and vorticity contours through the CFD-Post processing software, so as to clearly show the tanker wake effects on the trailing UAV, and lay a solid foundation to the later control algorithm design of the AAR technology.

2. NUMERICAL METHOD

2.1 Governing Equations

The ANSYS CFX 15.0 based on finite volume method is used to solve the following Navier-Stokes equations:

$$\frac{\partial(\rho u)}{\partial t} + \text{div}(\rho u \mathbf{u}) = \text{div}(\mu \text{grad } u) - \frac{\partial p}{\partial x} + S_u \quad (1)$$

$$\frac{\partial(\rho v)}{\partial t} + \text{div}(\rho v \mathbf{u}) = \text{div}(\mu \text{grad } v) - \frac{\partial p}{\partial y} + S_v \quad (2)$$

$$\frac{\partial(\rho w)}{\partial t} + \text{div}(\rho w \mathbf{u}) = \text{div}(\mu \text{grad } w) - \frac{\partial p}{\partial z} + S_w \quad (3)$$

where ρ is fluid density, t is time, \mathbf{u} is velocity vector, p is pressure of microelement in fluid, $\text{div}(\)$ is divergence, $\text{grad}(\)$ is gradient, S_u , S_v , S_w are generalized source terms of momentum conservation equations in u , v and w directions.

For turbulence, the instantaneous flow variables are decomposed into mean values and turbulence fluctuations by Reynolds averaging technique, and standard $k-\varepsilon$ equations (Görtz, 2003) are selected for turbulence model of flow field.

The autonomous aerial refueling altitude is set at 10 km, temperature is 223.3 K, pressure is 26500 Pa, density is 0.4135 kg/m³, and Reynolds number is 2.1×10^7 based on average aerodynamic chord length. The velocity inlet boundary condition is set to 0.7 Ma, outlet boundary is set as free outlet, and surface of the tanker and the trailing UAV is set as no-slip wall.

2.2 Geometry and Mesh

A simplified boom-equipped tanker and a flying wing UAV named ZD-X are used for simulation analysis to study the influence of tanker wake on the receiver. The tanker parameters are: the length is 40.36 m, height is 10.2 m, wingspan is 35.26 m, boom length is 14.4 m, and attack angle of tanker is set at 2 degrees. Parameters of ZD-X are depicted as follows: length is 10 m, height is 1.7 m, wingspan is 10.9 m, and attack angle of ZD-X is set at 3 degrees.

The numerical calculations are arranged as follows. In the longitudinal direction (x -axis), three spacings of 0.8b, 1.2b, and 2b are set up between tanker and ZD-X (b is tanker wing span). In the lateral direction (y -axis), there are ten spacings between the tanker and ZD-X, each is set to 0.1b. In the vertical direction (z -axis), there are four spacings between the tanker and ZD-X, each spacing is also set to 0.1b, a vertical spacing of 0 means that the trailing UAV is 0.35 m below the horizontal tail and wing tip of the tanker. All spacings represent the distance between the centers of gravity of the two vehicles. Fig. 1 shows the configuration and relative position of tanker and ZD-X.

All the numerical calculations in this paper use the unstructured tetrahedral grids, which are generated by ANSYS ICEM CFD 15.0 software. To verify sensitivity of the calculated results to the change of grid number, the model that the trailing UAV is located 18.504 meters behind the tanker is selected for calculation, that is, relative position of the two vehicles is $x/b=1.2$, $y/b=0$, $z/b=0$. The grid independence test is carried out by gradually refining the computational grids, especially the grids near the surface of tanker and trailing UAV and the flow field near the wing tip vortex. A total of six cases with different numbers of grids are generated, as shown in Table 1.

Fig. 2 shows the variation of lift coefficient of ZD-X with the increase of grid number. It can be seen

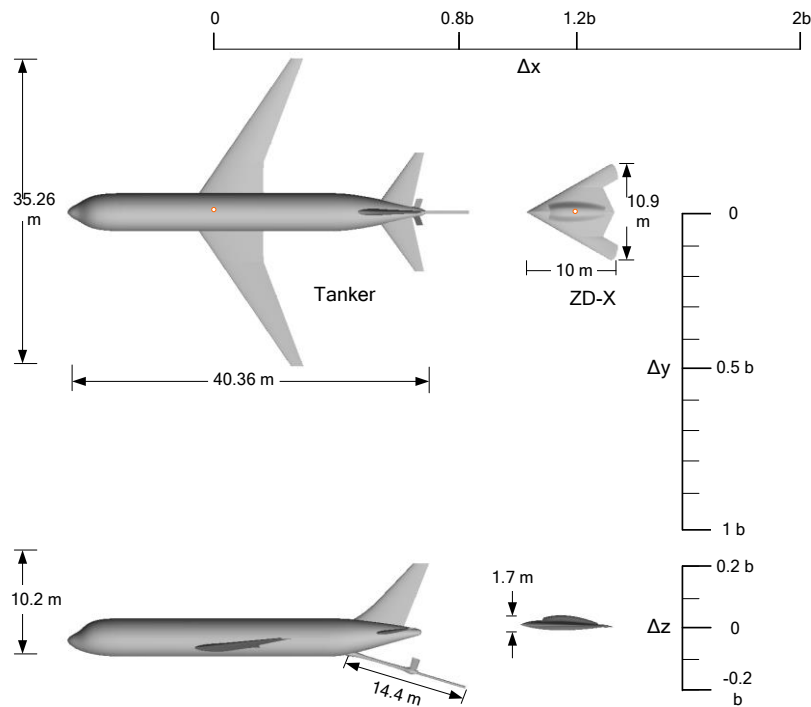


Fig. 1. Configuration and relative position of tanker and ZD-X.

that with the increase of grids number, the calculation value of lift coefficient changes more and more slowly. When the number of grids reaches 13 million, the variation of lift coefficient can be neglected. Fig. 3 shows the vorticity contours of wing tip vortices of the tanker with four different grid numbers. The captured wing tip vortices become more and more accurate with the increase of grids number. When the number of grids exceeds 13 million, it is difficult to see the difference of the vorticity contours under different grid numbers.

Based on the above analysis, the grid size and generation method of case E are used as the grid generation benchmark of all the computational models in this paper, which can not only satisfy the accuracy of calculation, but also save computing resources and computing time. The surface grids, near-wall grids and refined regions of the computational model in case E are shown in Fig. 4.

Table 1 Six cases with different numbers of grids

Case	Numbers of grids
A	5,240,423
B	7,153,712
C	9,050,078
D	11,053,712
E	13,125,241
F	15,230,983

2.3 Verification

The CT-1 model (Wang *et al.* 2008) is used to

verify the numerical simulation method. This section mainly compares the errors between the numerical results and wind tunnel test data at small attack angles, since the numerical calculation at high attack angles is not carried out in this paper. For the sake of clarity, only the lift and pitching moment of the CT-1 are compared. The configuration of the CT-1 is shown in Fig. 5, it is a fighter model with a tail strut. The calculation conditions are as follows: the angle of attack varies from -5 to 10 degrees, the inlet velocity of the flow field is set to 0.5 Ma, the Reynolds number is 1.4×10^6 based on average aerodynamic chord length, the outlet flow is set as free outlet, and the surface of the tanker and the trailing UAV is set as no-slip wall.

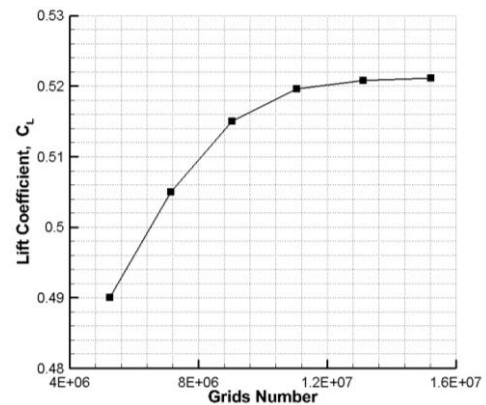


Fig. 2. Variation of lift coefficient of ZD-X with the increase of grids number.

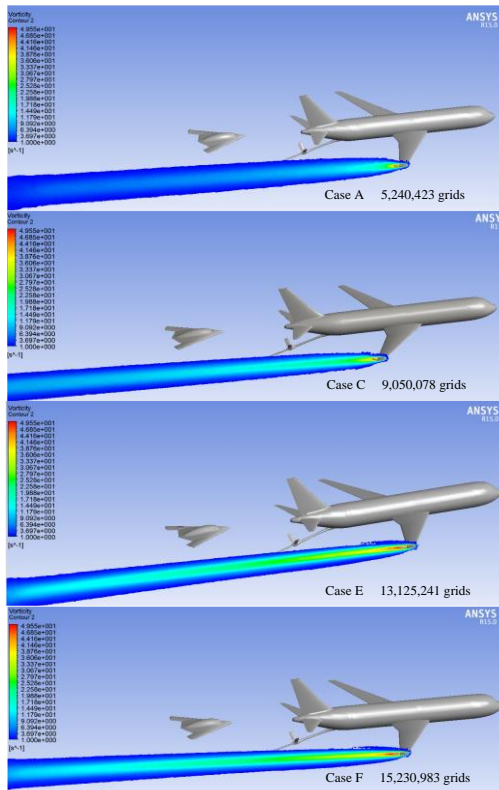
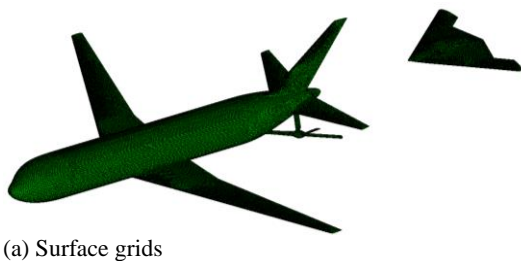
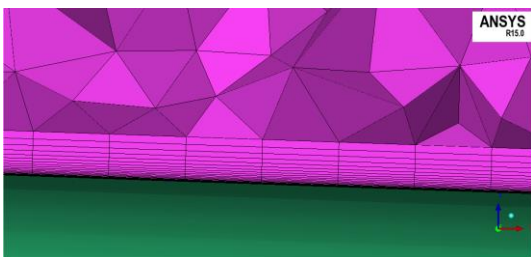


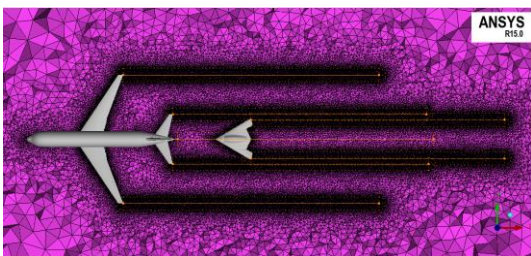
Fig. 3. Vorticity contours of wing tip vortices of the tanker with different grid numbers.



(a) Surface grids



(b) Near-wall grids



(c) Refined region

Fig. 4. Grids distribution of the computational model in case E.

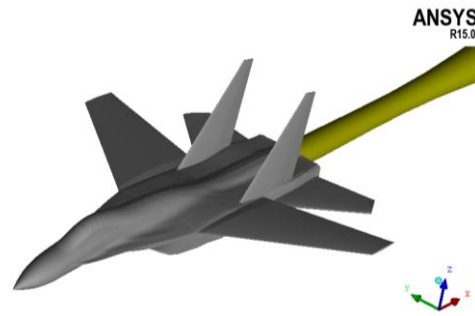
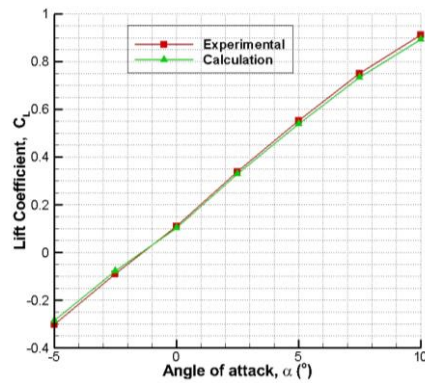
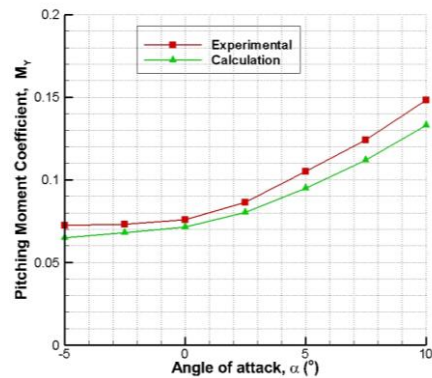


Fig.5. Configuration of the CT-1 model.



(a) Lift coefficient



(b) Pitching moment coefficient

Fig. 6. Comparisons between calculation and experimental values.

Fig. 6 shows the comparisons between calculation experimental values. The results show that calculation values of lift coefficient and pitch moment coefficient are slightly smaller than experimental values, and the error increases with the absolute value of attack angle. At 10 degrees of attack angle, maximum error of lift coefficient is 0.0182 and that of pitch moment coefficient is 0.015. When the angle of attack is between 2 and 3 degrees, the error of lift coefficient is only about 0.0045, and the error of pitch moment coefficient is about 0.0051, which means that the numerical calculation is very accurate in the range of the attack angle of the tanker and trailing UAV. The comparison results show that calculation values agree well with experimental values, which means that the numerical method is reliable for the study of this paper.

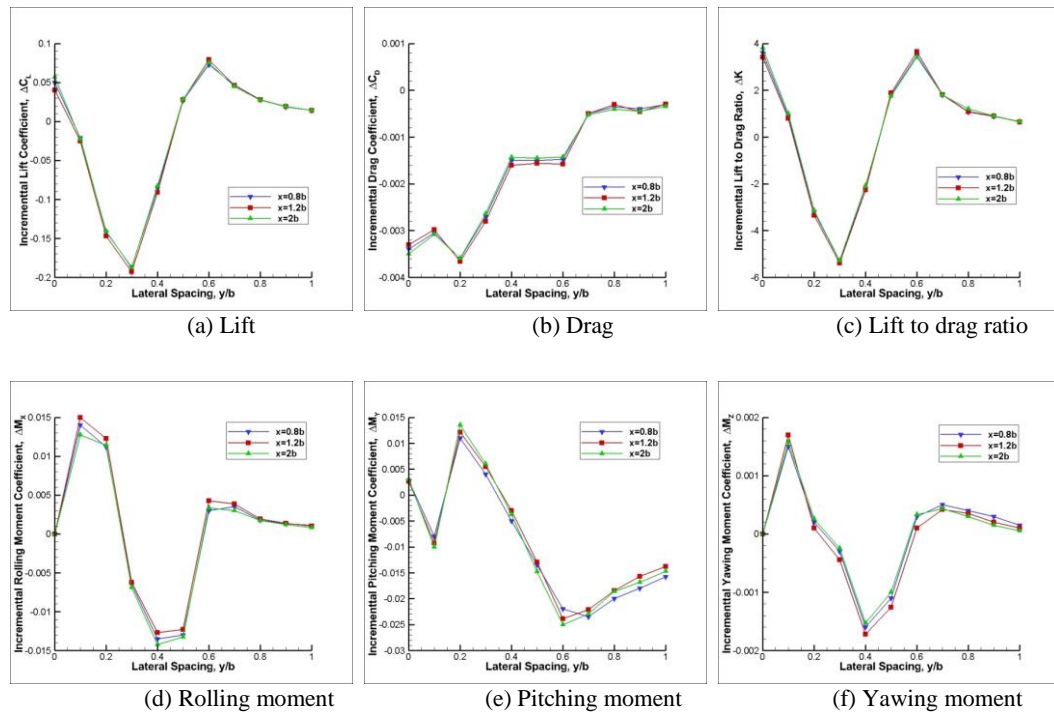


Fig. 7. Effects of lateral and longitudinal spacings on the aerodynamic characteristics of ZD-X, $z/b=0$.

3. RESULTS AND DISCUSSIONS

The aerodynamic forces and moments of ZD-X in single flight are calculated first. In this case, the UAV is not affected by the tanker wake. Table 2 shows the aerodynamic characteristics of ZD-X in single flight at the attack angle of 3 degrees, which are used as the benchmark for comparison. Then the aerodynamic characteristics of ZD-X under the effects of the tanker wake are calculated. By comparing with the results in Table 2, the final value is given in incremental form in Fig. 7 and Fig. 8. The positive value means higher than the result of ZD-X in single flight, while the negative value is lower than the result of ZD-X in single flight.

Fig. 7 shows the effects of lateral and longitudinal spacings on the aerodynamic characteristics of ZD-X. During the calculation, the tanker and ZD-X are flying at the same level, that is, the tailing UAV is 0.35 m below the horizontal tail of the tanker. It can be clearly seen from the results that effects of longitudinal spacings on the aerodynamic characteristics of ZD-X are very small, while lateral spacing has great effect. Fig. 8 shows the effects of vertical spacings on the aerodynamic characteristics of ZD-X. The longitudinal spacing between the tanker and ZD-X is fixed at 0.8b. The results show that the tanker wake has a strong effect on ZD-X when the ZD-X is 0.35 m below the horizontal tail of the tanker. When the vertical spacing increases, the tanker wake effect decreases. However, the variation trend of aerodynamic forces and moments increment of ZD-X at different vertical spacings is consistent. Fig. 9 shows the cross section

streamlines and pressure counter of the tanker and ZD-X. The flow field behind the tanker is very complex. When moving laterally, the ZD-X will encounter the cores of the vortex from the tanker wings and horizontal tail, where the swirling strength is strong and the direction of the vortex changes drastically.

All results from Fig. 7 and Fig. 8 show the lateral spacing has an intense effect on the aerodynamic characteristics of ZD-X, and the effect is most obvious when the tanker and ZD-X fly at the same level. Therefore, effects of lateral spacings on the aerodynamic interference mechanism of the tanker and ZD-X flying at the same altitude will be discussed and explained in detail in the next part.

Table 2 Aerodynamic characteristics of ZD-X in single flight

Attack angle	3°
C_L	0.4807
C_D	0.0302
K	15.9172
M_x	0
M_y	-0.1352
M_z	0

All the calculation results in Fig. 7 are based on such a condition that tanker and ZD-X are flying at the same level, that is, the ZD-X is 0.35 m below

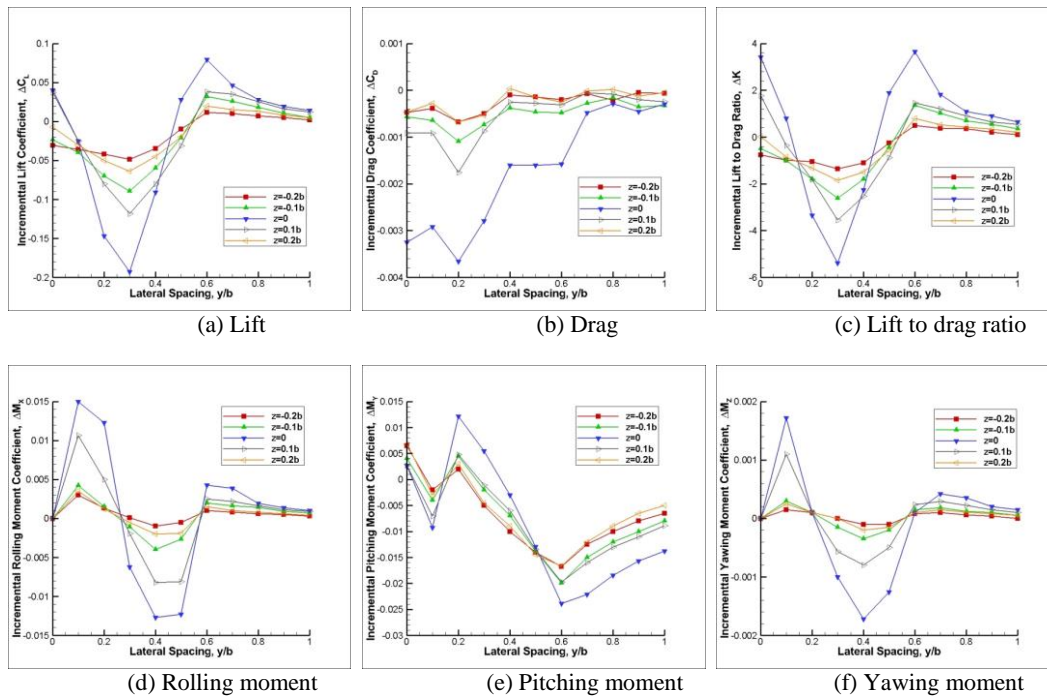


Fig. 8. Effects of vertical spacings on the aerodynamic characteristics of ZD-X.

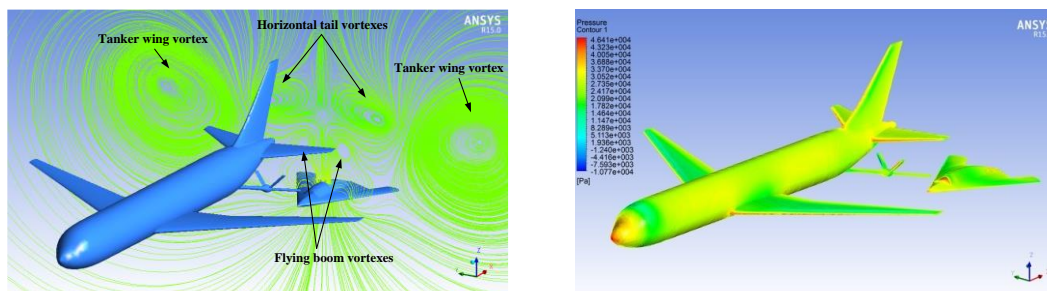


Fig. 9. Cross section streamlines and pressure counter of the tanker and ZD-X.

the horizontal tail of the tanker. The tanker wake effects on the aerodynamic forces of ZD-X are shown in Fig. 7(a-c). The variation of incremental lift coefficient and incremental lift-to-drag ratio of ZD-X is almost the same. With the centerlines of vehicles aligned ($y/b=0$), ZD-X is favorably affected by the tanker wake, lift coefficient of ZD-X is improved. As ZD-X moves outboard, the incremental lift coefficient diminishes and reaches minimum at $y/b=0.3$. Further outboard, the incremental lift coefficient increases and reaches maximum at $y/b=0.6$. As ZD-X moves more outboard, the incremental lift coefficient diminishes slightly. The drag coefficient of ZD-X decreases in all lateral spacings, and the minimum is obtained at $0.2b$ lateral spacing. As ZD-X moves from $0.2b$ to $0.4b$ lateral spacing, the drag coefficient increases sharply. Out of the wingtip of the tanker, there is a small drop in the drag coefficient of ZD-X.

Fig. 10 shows flow field structure and marks out the rotation directions of the vortices when ZD-X

located at $0.8b$ behind the tanker. Owing to the opposite of the attack angles, rotation directions of the vortices from the wing and horizontal tail are different. When located at $0.8b$ behind the tanker, wingtips of ZD-X are in the upwash flow from the horizontal tail vortices, so the lift coefficient increases. The variation of drag coefficient of ZD-X is complicated, which is mainly affected by two factors. One is the upwash and downwash of the tanker wake. The drag coefficient increases when the upwash is dominant and decreases when the downwash is dominant. Another factor is the strength of the wingtip vortices of the trailing UAV. The drag coefficient increases when the strength of the wingtip vortices of ZD-X is strengthened, and decreases when the strength is weakened. However, the strength of the wingtip vortices of ZD-X is mainly affected by the tanker wake. When ZD-X is aligned with the tanker at the relative position of $x=0.8b, y=0, z=0$, the upwash flow from the tanker wake increases the drag coefficient, but it correspondingly weakens the strength of wingtip

vortices of ZD-X, which reduces the drag coefficient. The drag coefficient decreases more than increase, so the drag coefficient of ZD-X decreases as a whole. Due to the increase of lift and decrease of drag, lift-to-drag ratio of ZD-X is greatly improved.

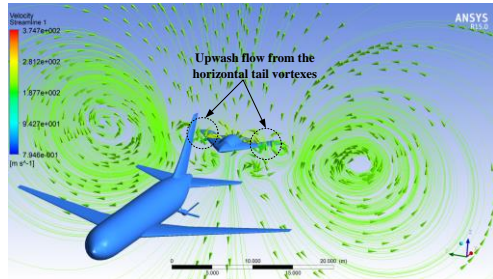


Fig. 10. Cross section streamlines, $y=0$.

When ZD-X is located at $0.3b$ lateral spacing, as shown in Fig. 11, downwash flow from horizontal tail and left wing of the tanker simultaneously affects ZD-X, so the lift coefficient diminishes to minimum. At $0.6b$ lateral spacing, almost all the wing and body of ZD-X are in the upwash flow from the left wing of the tanker (see Fig. 12), so the lift coefficient increased. The vortex core region of the tanker and ZD-X defined through swirling strength method is shown in Fig. 13. The swirling strength is imaginary part of complex eigenvalues of velocity gradient tensor (Martin *et al.* 1995). The vortex from ZD-X wingtip is weakened and inhibited by vortex from the left tanker wing, so the drag coefficient of ZD-X decreases. Fig. 14 shows the 3-dimensional streamlines from the two vehicles. The streamlines from the tanker rotate clockwise while the streamlines from ZD-X rotate counterclockwise, so the strength of ZD-X wingtip vortex is weakened, thus leads to a reduction of drag coefficient.

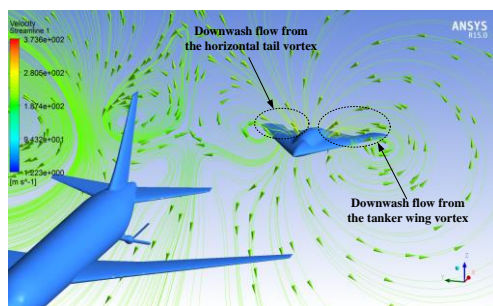


Fig. 11. Cross section streamlines, $y=0.3b$.

The tanker wake effects on the aerodynamic moments of ZD-X are shown in Fig. 7(d-f). When moving outboard, the rolling moment of ZD-X increases first and obtains maximum value at $0.1b$ lateral spacing, then it diminishes rapidly and changes sign at $0.25b$ lateral spacing. Further outboard, the rolling moment obtains minimum value at $0.4b$ lateral spacing. From $0.4b$ to $0.6b$ lateral spacing, the rolling moment of ZD-X increases again, and it decreases as ZD-X moves

more outboard and eventually approaches zero value.

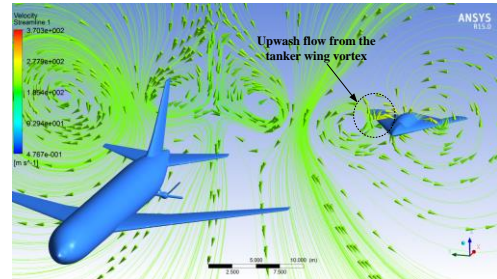


Fig. 12. Cross section streamlines, $y=0.6b$.

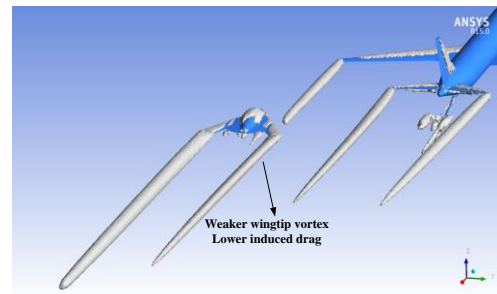


Fig. 13. Vortex core region of tanker and ZD-X.

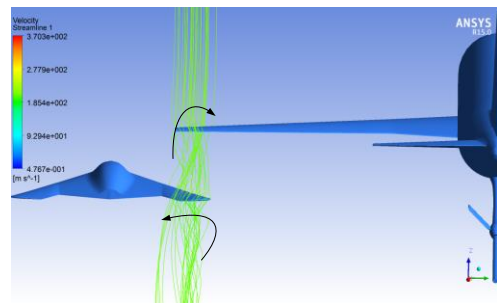


Fig. 14. Velocity streamlines of tanker and ZD-X.

Fig. 7(e) shows the tanker wake effects on the pitching moment of ZD-X. When ZD-X is aligned with the tanker, there is a slight nose-up pitching moment of ZD-X. The pitching moment changes to nose-down and then decreases when moving outboard. At $0.2b$ lateral spacing, ZD-X obtains maximum nose-up pitching moment. Further outboard, the nose-up pitching moment decreases and changes sign at about $0.35b$ lateral spacing. Out of the wingtip of the tanker, the nose-down pitching moment decreases because of the weakened tanker wake effect.

Fig. 7(f) shows the tanker wake effects on the yawing moment of ZD-X. The yawing moment is very small due to the lack of a vertical tail on the trailing UAV (Qu *et al.* 2017). When moving outboard, the nose-left yawing moment of ZD-X increases first and obtains maximum value at $0.1b$ lateral spacing, then it diminishes and reverses direction at $0.25b$ lateral spacing. More outboard, the nose-right yawing moment obtains maximum at

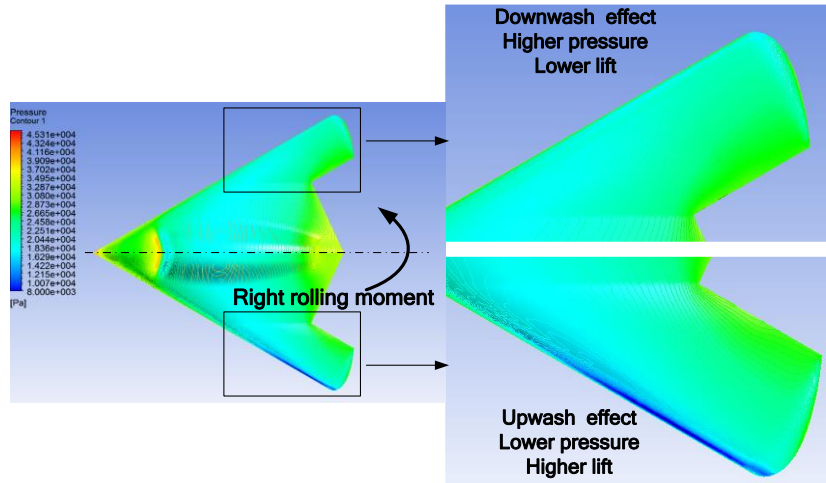


Fig. 15. Surface pressure contour of the trailing UAV, $x=1.2b$, $y=0.4b$, $z=0$.

0.4b lateral spacing. Further outboard, the nose-right yawing moment diminishes and eventually reverses direction. Out of the wingtip of the tanker, the nose-left yawing moment decreases and eventually approaches zero value.

All of the incremental aerodynamic moments are derived from unevenly distributed aerodynamic forces on ZD-X. Fig. 15 shows the surface pressure contour of ZD-X when the relative position to the tanker is $x=1.2b$, $y=0.4b$, $z=0$. Owing to the upwash effect from the tanker wake, a distinct low pressure zone appears on the upper surface of left wing, which increases its lift. Meanwhile, the lift on the right wing decreases due to the downwash effect from the tanker wake. Ultimately, the unbalanced lift distribution on ZD-X leads to the right rolling moment.

4. CONCLUSIONS

The tanker wake effects on receiver in the autonomous aerial refueling are studied through CFD method and the following conclusions are drawn:

- (1) The tanker wake effects on receiver mostly come from wingtip vortices of the tanker wing and horizontal tail.
- (2) Effects of longitudinal spacings on the aerodynamic characteristics of ZD-X are very small, while lateral spacing has a very large effect.
- (3) The tanker wake has a strong effect on ZD-X when the two vehicles fly at the same height, and the effect weakens with the increase of vertical spacing. However, the variation trend of aerodynamic forces and moments increment of ZD-X at different vertical spacings is consistent.
- (4) The incremental yawing moment coefficient of ZD-X is very small, but the tanker wake effects

on ZD-X may be great, because there is no traditional rudder control surface.

ACKNOWLEDGEMENTS

The authors gratefully acknowledge the financial supports by the National Natural Science Foundation of China (61473307).

REFERENCES

- Anon. Unmanned Aerial Vehicle (UAV) roadmap 2005-2030[M]. *Office of the Secretary of Defense*, 2005.
- Blake, W., E. G. Dickes and D. R. Gingras (2004) UAV aerial refueling-wind tunnel results and comparison with analytical predictions. In: *AIAA atmospheric flight mechanics conference and exhibit*, Providence, RI.
- Blake, W. and D. Gingras (2004) Comparison of predicted and measured formation flight interference effects. *Journal of Aircraft* 41(2):201-7.
- Bloy, A. W., Ali, K. and V. Trochalidis (1987) The longitudinal dynamic stability and control of a large receiver aircraft during air-to-air refueling. *Aeronautical Journal* (91):64-71.
- Bloy, A. W., P. J. Lamont, H. A. Abu-Assaf and K. A. M. Ali (1986) The lateral dynamic stability and control of a large receiver aircraft during air-to-air refueling. *Aeronautical Journal* (90), 237-43.
- Bloy, A. W. and V. Trochalidis (1990) The aerodynamic interference between tanker and receiver aircraft during air-to-air refueling. *Aeronautical Journal* (94):165-71.
- Bloy, A. W., M. G. West, K. A. Lea and M. Joumaa (1993) Lateral aerodynamic interference between tanker and receiver in air-to-air

- refueling. *Journal of Aircraft* 30(5), 705-10.
- Dogan, A., T. A. Lewis and W. Blake (2008) Flight data analysis and simulation of wind effects during aerial refueling. *Journal of Aircraft* 45(6), 2036-48.
- Dogan, A., S. Venkataramanan and W. Blake (2005) Modeling of aerodynamic coupling between aircraft in close proximity. *Journal of Aircraft* 42(4), 941-55.
- Fravolini, M. L., A. Ficola, G. Campa, M. R. Napolitano and B. Seanor (2004) Modeling and control issues for autonomous aerial refueling for UAVs using a probe-drogue refueling system, *Aerospace Science and Technology* 8(7), 611-618.
- Gerza, T., F. Holzapfel and D. Darracq (2002) Commercial Aircraft Wake Vortices, *Progress in Aerospace Sciences* 38, 181-208.
- Görtz, S. (2003) Detached-eddy simulations of a full-span delta wing at high incidence, in: *AIAA 21st Applied Aerodynamics Conference*, Orlando, FL, AIAA Paper 2003-4216.
- Martin, R. and P. Ronald (1998) A Higher-order Method for Finding Vortex Core Lines. *Proceeding of Conference on Visualization*.
- Qu, X., W. Zhang, J. Shi and Y. Lyu (2017) A novel yaw control method for flying-wing aircraft in low speed regime. *Aerospace Science and Technology* 69 636–649.
- Vachon, M. J., R. Ray, K. Walsh and K. Ennix (2003). F/A-18 Aircraft Performance Benefits Measured During the Autonomous Formation Flight Project[C]. *NASA TM-2003-210734*; September.
- Waharte, S. and N. Trigoni (2010) Supporting search and rescue operations with UAVs[C]. *IEEE International Conference on Emerging Security Technologies (EST)*, 142-147.
- Wang, Y, G. Wang and Z. Chen (2008) Numerical simulation of static aerodynamic characteristics of CT-1 model at high angles of attack[J]. *Chinese Journal of Aeronautics* 29(4):859-866.